Steering an actuated-tip needle in biological tissue

Fusing FBG-sensor data and ultrasound images

Shahriari, N.; Roesthuis, RJ; Van De Berg, Nick J.; Van Den Dobbelsteen, John J.; Misra, S

Citation (APA)
Shahriari, N., Roesthuis, RJ., Van De Berg, N. J., Van Den Dobbelsteen, J. J., & Misra, S. (2016). Steering an actuated-tip needle in biological tissue: Fusing FBG-sensor data and ultrasound images. In *Proceedings of the IEEE International Conference on Robotics and Automation: ICRA 2016* (pp. 4443-4449). Article 7487644 IEEE. https://doi.org/10.1109/ICRA.2016.7487644

Important note
To cite this publication, please use the final published version (if applicable).
Please check the document version above.

Steering an Actuated-Tip Needle in Biological Tissue: Fusing FBG-Sensor Data and Ultrasound Images

Navid Shahriari, Roy J. Roesthuis, Nick J. van de Berg,
John J. van den Dobbelsteen and Sarthak Misra

Abstract— Needle insertion procedures are commonly performed in current clinical practice for diagnostic and therapeutic purposes. Although prevailing technology allows accurate localization of lesions, they cannot yet be precisely targeted. Needle steering is a promising technique to overcome this challenge. In this paper, we describe the development of a novel steering system for an actuated-tip flexible needle. Strain measurements from an array of Fiber Bragg Grating (FBG) sensors are used for online reconstruction of the needle shape in 3D-space. FBG-sensor data is then fused with ultrasound images obtained from a clinically-approved Automated Breast Volume Scanner (ABVS) using an unscented Kalman filter. A new ultrasound-based tracking algorithm is developed for the robust tracking of the needle in biological tissue. Two experimental cases are presented to evaluate the proposed steering system. In the first case, the needle shape is reconstructed using the tracked tip position in ultrasound images and FBG-sensor measurements, separately. The reconstructed shape is then compared with the actual 3D needle shape obtained from the ABVS. In the second case, two steering experiments are performed to evaluate the overall system by fusing the FBG-sensor data and ultrasound images. Average targeting errors are 1.29±0.41 mm and 1.42±0.72 mm in gelatin phantom and biological tissue, respectively.

I. INTRODUCTION

Percutaneous needle insertion is a common minimally invasive surgical procedure. Needle interventions are used for both diagnostic and therapeutic purposes such as biopsy and ablation, respectively. Clinicians use various imaging modalities, such as computed tomography (CT), magnetic resonance imaging (MRI) and ultrasound to reach the target accurately. Current imaging technology can provide accurate localization of lesions. However, precise targeting of the lesions by manual insertion of rigid needles is both difficult and time-consuming [1]. The clinicians' experience and lesion location are two factors which affect the targeting accuracy, and therefore influence the number of attempts for a successful insertion. Rigid needles have only limited

N. Shahriari, R. J. Roesthuis and S. Misra are affiliated with the Surgical Robotics Laboratory, Department of Biomechanical Engineering (MIRA-Institute for Biomedical Technology and Technical Medicine), University of Twente, The Netherlands {n.shahriari, r.j.roesthuis, s.misra}@utwente.nl.

N. Shahriari and S. Misra are also affiliated with the Center for Medical Imaging - North East Netherlands, University Medical Center Groningen, University of Groningen, The Netherlands.

N. J. van de Berg and J. J. van den Dobbelsteen are affiliated with the Department of Biomechanical Engineering (3mE), Delft University of Technology, The Netherlands {n.j.p.vandeberg, j.j.vandendobbelsteen}@tudelft.nl.

S. Misra is also affiliated with the Department of Biomedical Engineering, University Medical Centre Groningen, University of Groningen, The Netherlands.
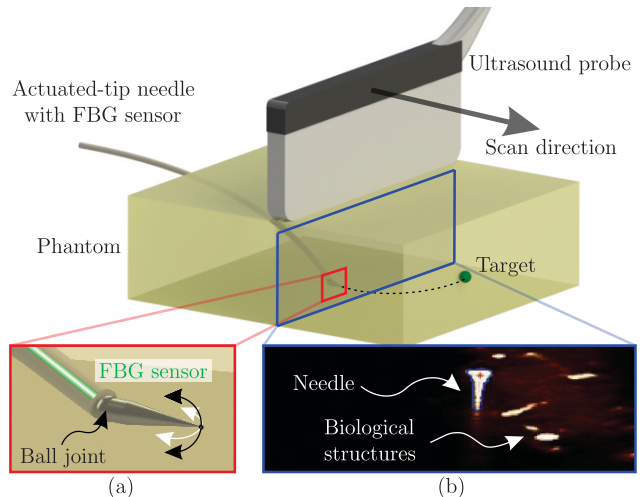
Fig. 1. A flexible actuated-tip needle is steered in biological tissue (chicken breast) towards a real target. Fiber Bragg grating (FBG) sensors are used to reconstruct the needle shape. The needle tip is tracked using an ultrasound transducer. The tip position from ultrasound images is fused with FBG-sensor data using an unscented Kalman filter. The estimated tip position is provided to the steering algorithm as feedback. (a) The actuated-tip needle (b) An ultrasound image showing the needle radial cross-section and biological structures.

steering capabilities, and it is difficult to compensate for targeting errors during insertion. Flexible needles have the benefit that they can travel on a non-straight path which provides more control over the needle trajectory with respect to rigid needles.

A. Related work

1) Needle steering: Various flexible needle designs have been developed for steering, and those can be divided into two categories: Passive and active. Passive needles have a pre-defined shape, and steering is achieved by controlling the base motion of the needle. Needles with symmetric, beveled and pre-bend/curved tips are passive needles that have been used in many studies [2]–[4]. Active needles can change their shape, either at the tip or along the entire length. Examples of active needles are concentric tubes [5], [6], pre-curved stylet [7], programmable bevel [8] and tendon-actuated tip [9], [10] needles. Passive needles need to be rotated along their longitudinal axis in order to control their path through the soft tissue. The rotation of the needle may cause tissue damage [11]. On the other hand, active needles can be steered in any direction without rotating the needle along its longitudinal axis. In our previous work, we presented a novel
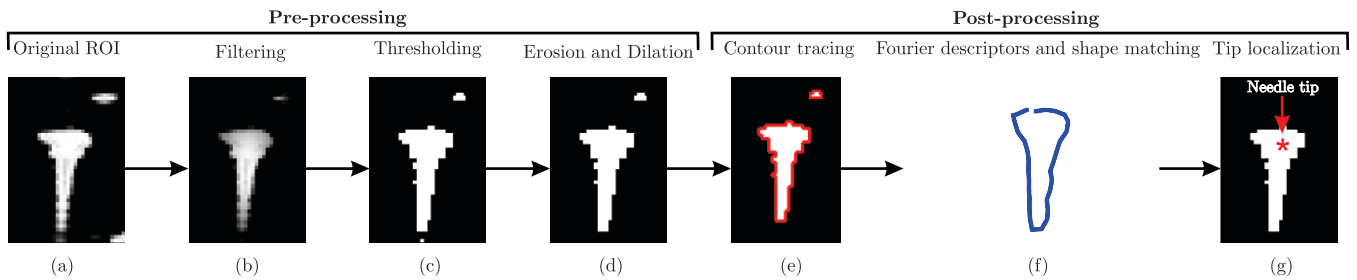
Fig. 2. The image processing method used to detect and localize the needle tip position using ultrasound images: (a) The region-of-interest (ROI) is selected automatically based on the estimated needle tip position. (b) The ROI is filtered to reduce the noise. (c) The ROI is converted to a binary image by thresholding. (d) Speckles are removed using erosion and dilation. (e) The contours of remaining objects are traced. (f) Fourier descriptors for the contours are calculated, normalized and then compared with the preoperative sampled data, and the needle is detected. (g) The needle tip is localized.

actuated-tip needle and developed a model and a controller to steer the needle [9]. Fiber Bragg Grating (FBG) sensors were used to reconstruct the needle shape. FBG-sensor data were then used to close the control loop. The overall system was used to steer towards virtual targets in gelatin phantoms.

Preliminary studies have demonstrated that steering is challenging in biological tissue, because the tissue is heterogeneous and the needle deflection varies in different parts of the tissue [12]. In this work, we are moving our research towards more clinically-relevant conditions. We are using biological tissue (chicken breast) as our test medium and ultrasound images are combined with FBG measurements to track the needle in 3D and steer it towards a real target.

2) Needle tracking: Ultrasound is a safe and easily accessible imaging modality which is commonly used for various clinical interventions such as breast and prostate biopsy [13], [14]. Previous studies have used 2D ultrasound images to insert the needle within the 2D plane of the ultrasound transducer [2], [15]. Neshat and Patel developed a system to track a curved needle in 3D space by rotating a 2D ultrasound transducer about its axis [16]. However, the tracking was tested only in an agar. Chatelain *et al.* proposed a method to detect the needle using 3D ultrasound images [17]. The method is limited to rigid needles and has not been tested in biological tissue. Pourtaherian *et al.* developed a tracking method which locally searches for the axis that appears more bright following a Gradient Descent strategy [18]. This method was evaluated using 3D ultrasound images, however, it is applicable only for rigid needles. Most studies use soft-tissue simulants made from homogeneous gelatin phantoms, in which the needle can be easily located from the ultrasound images. Vrooijink *et al.* attached an ultrasound transducer to a Cartesian robot [12], [19]. They combined 2D ultrasound images with transducer position feedback to track the needle in 3D, both in gelatin phantoms and in biological tissue. It was shown that needle detection and tracking in biological tissue is more challenging than in gelatin phantoms. Anatomical structures can be easily detected as the needle tip, or they may even completely mask the needle tip in the ultrasound image (Fig. 1(a)). Therefore, new techniques are needed in order to locate the needle robustly in biological tissue.

Several studies have used FBG sensors to determine deflected needle shapes during insertion into soft tissues [20],

[21]. Accurate reconstruction of needle shape has been demonstrated using this method. However, additional imaging modalities are required in order to relate the position of the deflected needle shape with respect to a target in the soft tissue. Therefore, it is necessary to fuse the FBG-sensor data with an additional imaging data. We have proposed a new tracking algorithm that uses fused ultrasound images and FBG-sensor data to locate the needle tip. This method enables robust tracking of the needle tip in biological tissue.

B. Contributions

This paper presents a novel system to track and steer a flexible actuated-tip needle in biological tissue towards a real target. The reconstructed needle shape from FBG measurements is fused with the tracked needle tip position from ultrasound images using an unscented Kalman filter. A novel image processing algorithm, along with previously mentioned data fusion, enables robust tracking of the needle in biological tissue in the presence of anatomical structures. A clinically-approved automated ultrasound transducer (Automated Breast Volume Scanner (ABVS)) is used to validate the proposed tracking and steering algorithms. The ABVS is also used pre-operatively to register the target location in the needle tip frame, which enables steering towards a real target. The combination of a clinically-approved imaging device and an advanced needle steering system is a step towards bringing robotic needle steering into clinical practice.

The paper is organized as follows. Section II describes the method developed for needle tracking and steering. The experimental setup, plan and results are presented in section III. Finally, in section IV, we conclude our work and suggest directions for future work.

II. METHODS

This section presents the technique developed for real-time tracking and steering of an actuated-tip needle. Ultrasound images are fused with FBG-sensor data to provide needle tip pose as feedback to the steering algorithm.

A. Shape sensing using Fiber Bragg Grating sensors

FBG sensors are optical strain gauges. The change in the reflected Bragg wavelength is related to the mechanical strain applied to the fiber [22]. FBG sensors can measure
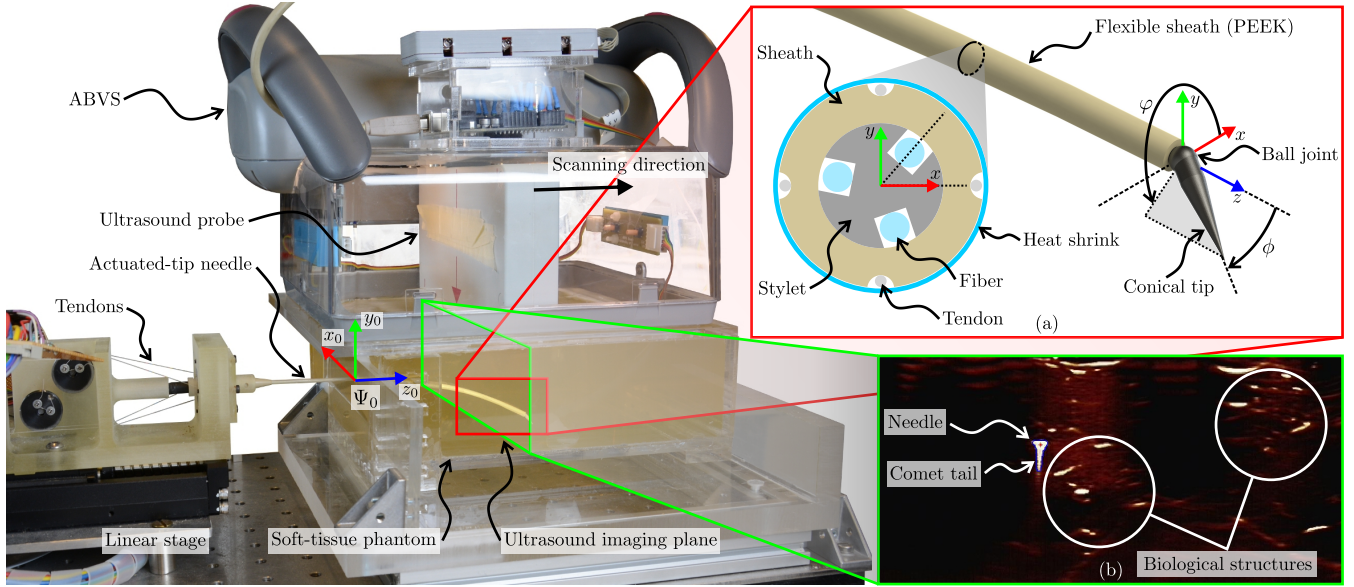
Fig. 3. The experimental setup consists of a flexible needle which is mounted on a linear stage to enable insertion into biological tissue (chicken breast). (a) The flexible needle has an actuated-tip, consisting of a conical tip mounted on a ball joint. Actuated-tip orientation is defined by the steering direction angle (φ), and the steering angle (ϕ). The tip is actuated by four tendons, which run through the outer sheath and are held in place by heat shrink. The stylet is made of a Nitinol wire (diameter 1 mm), in which three optical fibers are integrated in grooves. (b) An Automated Breast Volume Scanner (ABVS) is used to track the needle tip during insertion using ultrasound images.

the bending strain of the needle when positioned along the longitudinal axis of the needle. The magnitude and the direction of the bending curvature are determined using strain measurements from three co-located FBG sensors. Interpolation of the discrete curvature values is performed in order to approximate the curvature along the entire needle shaft. Finally, needle shape is reconstructed by integrating the curvature twice. For further details regarding shape reconstruction, we refer the reader to our previous study [20]. Steering of an actuated-tip needle using the reconstructed shape from FBG sensors towards virtual targets was performed in previous work [9], [10]. In this work, the reconstructed shape from FBG measurements is combined with ultrasound-based needle tracking to enable steering towards real targets.

B. Ultrasound-based needle tracking

This section presents the technique developed to detect and track a flexible needle in ultrasound images. The ultrasound transducer is placed perpendicularly to the needle insertion direction. Therefore, the images show a 2D radial cross-sectional view of the needle, which is circular (Fig. 2(a)). However, due to the reverberation artifact, a tail-shaped structure appears in the images [23]. The needle can be masked while it passes through certain parts of biological tissues, and biological structures can be incorrectly identified as the needle. An image processing algorithm (Fig. 2) along with an unscented Kalman filter (UKF) is used to overcome these problems.

The image processing is divided into pre-processing and post-processing phases. The pre-processing includes several basic image processing techniques (Fig. 2(b)-(d)). First, the

region-of-interest (ROI) is selected, based on the estimated needle tip position. This is followed by Gaussian filtering of the ROI. A 2D Gaussian matched filter is then applied, and the image is converted into a binary image by thresholding. The Gaussian filter parameters and the threshold value are evaluated using pre-operative trials. Erosion and dilation are used after that to eliminate speckles. The output of pre-processing is an enhanced and speckle-free binary version of original ROI.

The post-processing phase includes contour tracing, shape matching and tip localization (Fig. 2(e)-(g)). The contours of the objects in the ROI are traced using the OpenCV library [24]. The contours are then interpolated to 32 equally spaced points. Fourier descriptors are used to compare the shape of detected objects with a sample of the needle shape. The contour can be represented in a complex continuous form ($z \in \mathbb{C}^{32 \times 1}$) of:

$$z(s) = x(s) + \mathbf{j}y(s), \qquad (1)$$

where s is the arc length and $\mathbf{j}$ is the imaginary unit. x and y are contour points in pixels. The Fourier descriptors ($Z \in \mathbb{C}^{32 \times 1}$) are defined as:

$$Z_k = \frac{1}{P} \int_{s=0}^{P} z(s)\exp\left(\frac{-2\pi\mathbf{j}ks}{P}\right) \mathrm{d}s \quad (k = 0, \ldots, 31), \qquad (2)$$

where P is the perimeter of the contour. The Fourier descriptors are then normalized for position, size and starting point. The Fourier descriptors are computed for each of the interpolated boundaries. The normalized Fourier descriptors for a sampled needle shape are also computed before the experiment. The object with the most similar Fourier descriptor to the sampled shape is considered to be the needle.

To localize the needle tip, we assume that the needle's cross-section image is symmetric. The needle tip is placed at the center of the shape horizontally and it is located at a distance equal to the radius of the needle from the top of the shape (Fig. 2(g)).

C. Actuated-tip needle: Modeling and steering

The actuated tip needle consists of a conical tip, mounted on a ball joint [9], [10]. A set of four tendons are routed through the shaft of the needle and are attached to the conical tip, which enables changing of the actuated-tip orientation. Actuated-tip orientation is defined by two angles: The steering direction of the needle is defined by an angle (φ), while the steering angle (ϕ) determines the extent of needle bending (Fig. 3(a)).

Webster *et al.* developed a model based on the non-holonomic kinematics of a bicycle for flexible needles with a bevel tip [3]. A fixed steering constraint is used, which results in a needle path with a constant radius. The model is based on the bicycle model, but has been adapted in order to describe 3D motion for a needle with an actuated-tip (Fig. 3). The position and orientation of the needle tip ($\boldsymbol{p}_t \in \mathbb{R}^{3 \times 1}$) are represented in the rear frame (Ψ_r). The orientation of the front frame (Ψ_f) is defined by the actuated-tip orientation. The front frame has an offset (l) from the rear frame, along the z-axis of the rear frame, such that the radius of the needle path is given by:

$$r_r = l / \tan(\phi), \tag{3}$$

where ϕ is the steering angle of the actuated tip. The tissue surrounding the needle prevents sideways motion of the needle, resulting in four Pfaffian constraints for the model (velocities of the rear frame and front frame in the x-direction and y-direction are zero). Applying these constraints and choosing the rear frame velocity as the needle insertion velocity (v) results in the following kinematic model [9]:

$$\dot{\boldsymbol{q}} = \begin{bmatrix} \cos(\beta)\sin(\alpha) \\ \sin(\beta) \\ \cos(\alpha)\cos(\beta) \\ \frac{\cos(\varphi)\tan(\phi)}{l\cos\beta} \\ \frac{\tan(\phi)\sin(\varphi)}{l} \\ 0 \\ 0 \end{bmatrix} v + \begin{bmatrix} 0 \\ 0 \\ 0 \\ 0 \\ 0 \\ 1 \\ 0 \end{bmatrix} \dot{\varphi} + \begin{bmatrix} 0 \\ 0 \\ 0 \\ 0 \\ 0 \\ 0 \\ 1 \end{bmatrix} \dot{\phi}, \tag{4}$$

where α and β denote the orientation of the rear frame (Ψ_r) with respect to the global y-axis and x-axis (frame (Ψ_0)), respectively.

To steer the needle tip towards a target, the orientation of the actuated tip (i.e., φ and ϕ) needs to be calculated during insertion. Given the orientation of the needle at the tip (i.e., α and β) and the target position, the actuated-tip orientation can be calculated using trigonometry [9]. For this calculation, we assume the needle tip follows a circular path towards the target, as described by the model.

D. Data fusion using unscented Kalman filter

We have used UKF to fuse ultrasound and FBG noisy measurements, and to estimate the needle tip pose in 3D. UKF is a powerful tool for multi-sensor data fusion [25]. The state estimation is based on the process model, measurement model and measurements, similat to a standard Kalman filter. However, unlike the extended Kalman filter and other Taylor series-based approximation, Jacobian and Hessian matrices are not needed for the unscented transformation [26]. The UKF uses the unscented transformation for nonlinear sampling and propagation of state variables and nonlinear measurements.

The state vector of the actuated-tip needle is given by:

$$\boldsymbol{q} = \begin{bmatrix} p_{r,x}^0 & p_{r,y}^0 & p_{r,z}^0 & \alpha & \beta & \varphi & \phi \end{bmatrix}^T \in \mathbb{R}^{7 \times 1}, \tag{5}$$

where $p_r^0 = [p_{r,x}^0 \ p_{r,y}^0 \ p_{r,z}^0]^T \in \mathbb{R}^{3 \times 1}$ is the position of the rear frame (Ψ_r) represented in the global frame (Ψ_0). The process model is defined as:

$$\boldsymbol{q}_k = f(\boldsymbol{q}_{k-1}, \boldsymbol{u}_k) + \boldsymbol{w}_k, \tag{6}$$

where $\boldsymbol{u}_k$ is the vector of input velocities v, $\dot{\varphi}$ and $\dot{\phi}$. The function $f : \mathbb{R}^{10 \times 1} \rightarrow \mathbb{R}^{7 \times 1}$ is based on eq. (4), and $\boldsymbol{w}_k \in \mathbb{R}^{7 \times 1}$ is the process noise vector. The subscript k denotes the discrete time (i.e., $\boldsymbol{q}_k = \boldsymbol{q}(t_k)$). The measurement model:

$$\boldsymbol{z}_k = h(\boldsymbol{q}_k) + \boldsymbol{v}_k, \tag{7}$$

relates the current estimate of state with the measurement variable ($\boldsymbol{z}_k \in \mathbb{R}^{9 \times 1}$) through measurement function $h : \mathbb{R}^{7 \times 1} \rightarrow \mathbb{R}^{9 \times 1}$. The measurement noise ($\boldsymbol{v}_k \in \mathbb{R}^{9 \times 1}$) is assumed to be white Gaussian whose covariance depends on measurement accuracy. Ultrasound measures the tip position in the xy-plane with respect to the global frame (Ψ_0). FBG sensors are used to estimate the complete state vector of the needle ($\boldsymbol{q}$) by reconstructing the shape. $\boldsymbol{z}_k$ is the augmented vector of both measurements. UKF fuses all measurements to estimate the states of the system.

III. EXPERIMENTS

This section describes the experiments conducted. The proposed tracking, data fusion and steering algorithms are evaluated through experiments in both gelatin phantoms and biological tissue.

A. Experimental setup

The experimental setup which is used to validate the proposed algorithm is shown in Fig. 3. The actuated-tip needle is controlled through four steering tendons working in complementary pairs. The tendons are controlled by four Maxon ECmax 22 motors (Maxon Motor Ag., Sachseln, Switzerland). The needle consists of a Poly-Ether Ether Ketone (PEEK) plastic cannula (IDEX Health & Science, Oak Harbor, USA), with a diameter of 2 mm. Within the cannula, there is a nitinol stylet with a diameter of 1 mm. Three optical fibers are integrated in the wire, each having an array of four FBG sensors. The needle is attached to a linear stage which controls the needle insertion.
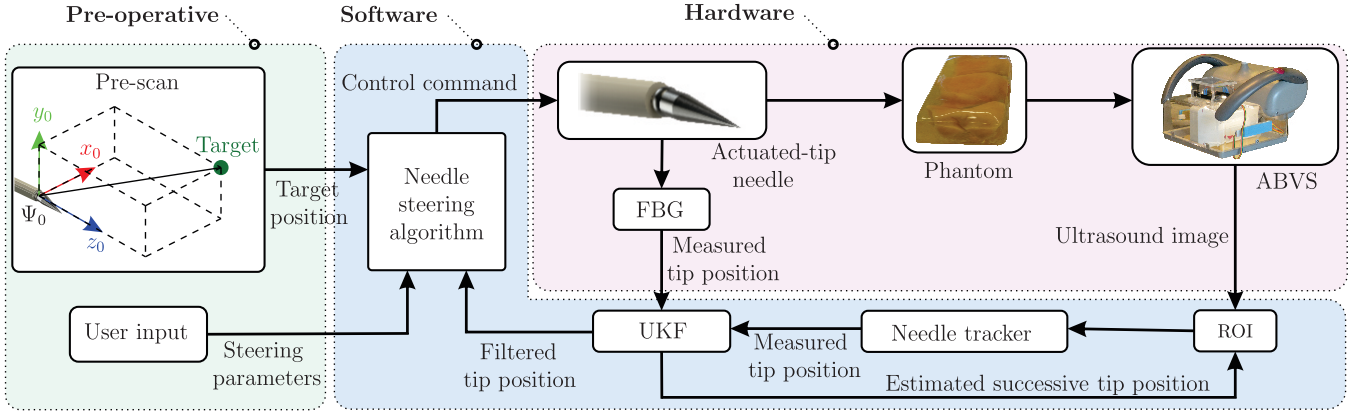
Fig. 4. Block diagram of the steering procedure: A pre-scan is performed using the Automated Breast Volume Scanner (ABVS) to register the target location in global frame (Ψ_0). Steering parameters (such as front frame offset (l) and maximum tip velocity) are set in the algorithm through the user input. The needle tip is tracked during insertion using the ABVS. The needle shape is reconstructed using Fiber Bragg Grating (FBG) sensors. Ultrasound and FBG measurements are fused using an unscented Kalman filter (UKF). Filtered measurements are used to update the region of interest (ROI) and to calculate the control commands in needle steering algorithm.

The ultrasound system is a Siemens Acuson S2000 (Siemens AG, Erlangen, Germany). The transducer is an Automated Breast Volume Scanner (ABVS) which is used for breast diagnosis. The transducer works at a frequency of 14 MHz and the resolution is 0.21 mm and 0.26 mm in the axial and sagittal planes, respectively. The ultrasound images are transmitted to the computer in real-time via a frame grabber at a rate of 11 Hz, which is the maximum frame rate allowed by the ABVS.

The ABVS scans the phantom at a constant speed of 1.55 mm/s. The needle insertion speed is synchronized with the ABVS speed to keep the needle tip within the ultrasound plane. This is achieved by defining two different insertion speeds. The needle is inserted at a speed of 1.4 mm/s if the needle is ahead of the transducer, and is therefore visible in ultrasound images. It is inserted at a speed of 1.7 mm/s if the needle is not visible in ultrasound images. This ensures that the needle tip is being tracked, not the needle shaft. The position of the transducer, and therefore the needle tip, is computed using linear stage motor encoder values. The needle velocity out of ultrasound plane is considered and compensated in the controller.

Gelatin phantoms and biological tissues are used in the experiments. The gelatin phantom is made by mixing 14.9% (by-weight) porcine gelatin powder (Dr. Oetker, Ede, The Netherlands) with 85.1% water. This mixture results in a phantom with a Young's modulus of 35 kPa, which is the elasticity of a normal woman's breast [27]. Biological tissue (chicken breast) is embedded in gelatin phantom to fixate it during experiments. Targets are made using 2% (by-weight) agar powder (VWR International BVBA, Leuven, Belgium) mixed with 98% water.

B. Experimental plan

Two experimental cases are used to evaluate the proposed tracking and steering algorithms (Section II). The experimental plan is described below.

Case I: The first experimental case is used to evaluate the accuracy of the proposed ultrasound-based tracking method. The needle shape is reconstructed using the real-time needle tip tracking data, and FBG-sensor measurements separately. The reconstructed shape is compared with the 3D volume output from the ABVS obtained from the same scan. Two sets of experiments are performed for this experimental case. Needle insertions in gelatin phantoms are performed along a straight path (Case I.A) and a curved path (Case I.B). The needle is inserted for 70 mm in both experiments. The steering angle (ϕ) is fixed at 0° and 15° for Case I.A and Case I.B, respectively.

Case II: In the second experimental case, the needle is steered towards a real target using the control scheme shown in Fig. 4. A pre-operative scan is performed by the ABVS to calculate the relative position of the target with respect to the global frame (Ψ_0). The needle tip position from ultrasound images and FBG-based reconstruction are fused to estimate the needle tip pose, which is used as feedback in the steering algorithm. Needle steering is performed in both gelatin phantoms (Case II.A) and biological tissue (Case II.B).

C. Results

The experimental Case I is evaluated by averaging the absolute distance between the reconstructed needle shape and the ABVS 3D volume (ground truth). ABVS data is manually

TABLE I
COMPARISON BETWEEN ULTRASOUND AND FIBER BRAGG GRATING (FBG) DATA: MEAN OF THE ABSOLUTE DISTANCE BETWEEN THE NEEDLE RECONSTRUCTED SHAPE AND AUTOMATED BREAST VOLUME SCANNER (ABVS) DATA: CASE I.A-STRAIGHT PATH, CASE I.B-CURVED PATH.

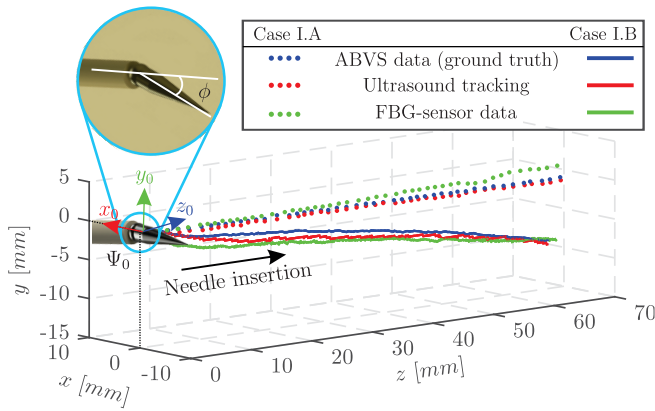| Experimental case	Ultrasound tracking	FBG sensor
Case I.A	$0.40 \pm 0.19\ mm$	$1.09 \pm 0.24\ mm$
Case I.B	$0.48 \pm 0.11\ mm$	$1.62 \pm 0.32\ mm$

Fig. 5. Results of a representative experiment for Case I.A (straight path, $\phi = 0$) and Case I.B (curved path, $\phi = 15$): The needle is inserted into a gelatin phantom with a steering angle ϕ. Automated Breast Volume Scanner (ABVS) data is considered as the ground truth. Fiber Bragg Grating (FBG) sensor data and our proposed ultrasound tracking data are compared with the ground truth. The error is calculated as the average absolute distance between the reconstructed needle shape and ABVS data. The global frame (Ψ_0) is defined at the initial needle position.

segmented to reconstruct the needle shape. Each experiment was repeated 5 times, and the results are presented in Table I. Experimental results show that a sub-millimeter tracking accuracy is obtained. The contact between the ultrasound transducer and the tissue causes deformations in the tissue, and thus the needle. Such deformations result in errors in calibration and reconstruction of FBG sensors. However, the results are improved by minimizing the contact force between the ultrasound transducer and the tissue. A representative reconstructed needle shape is shown in Fig. 5.

Case II is evaluated by the targeting error, which is calculated as the absolute distance between the target position and needle tip position. The average insertion depths are 102.1 mm and 100.8 mm for Case II.A and Case II.B, respectively. The targets are spheres with diameters ranging from 3 mm to 8 mm. The needle is steered towards the center of the targets. The steering parameters (such as front frame offset (l) and maximum tip velocity) are identical in Case II.A and Case II.B. The mean targeting errors are 1.29±0.41 mm and 1.42±0.72 mm for Case II.A and Case II.B, respectively. The results show that the targeting error increases when steering in biological tissue due to its inhomogeneity. The needle path is shown in Fig. 6 for the two steering experiments. The biological tissue experiments show that the needle tracking is able to distinguish between the needle and biological tissue structures. In a total of five experiments, the needle was masked seven times, and the tracker was able to detect the needle in all cases using the fused data. The accompanying video demonstrates an example of experimental Case II.A-B and the results of the steering experiments.

IV. CONCLUSIONS AND FUTURE WORK

This paper has presented a novel system to steer a flexible actuated-tip needle by fusing FBG-sensor data and ultrasound images. The needle is equipped with 12 FBG sensors, which are used to reconstruct the needle shape. The needle tip is tracked by a clinically-approved automated ultrasound transducer during insertion. The tip position measurements using FBG sensors and ultrasound images are fused using an unscented Kalman filter. Adding an imaging system to FBG-based reconstruction is crucial to register the target position with respect to the global frame. The imaging system is also used to evaluate the targeting accuracy. On the other hand, FBG-sensor data help to track the needle tip when the needle is masked by anatomical structures in ultrasound images. The proposed method is evaluated by two experimental cases. The first experimental case focuses on evaluating the accuracy of our proposed tracking algorithm. The needle is steered towards real targets in gelatin phantoms and biological tissue in the second experimental case.

A. Conclusions

The first experimental case validates the accuracy of the proposed ultrasound-based tracking. The results for Case I.B show that the ultrasound-based reconstruction error (0.48 ± 0.11 mm) is less than FBG-based reconstruction (1.62 ± 0.32 mm). The second experimental case (steering experiment) shows that the targeting accuracy is higher in gelatin phantoms (1.29±0.41 mm) than in biological tissue (1.42±0.72 mm). This is due to the fact that the tissue is homogeneous and the needle kinematic model can predict the behavior of the needle more accurately than it can in biological tissue. The needle was masked 7 times in biological tissue experiments, and the ultrasound-based tracking was able to detect the needle in successive images in all cases by using the fused data.

B. Future work

Although the current study has addressed some of the challenges in the needle steering domain, we believe the results can be further improved in future work. Pre-operative path planning can help in defining the suitable insertion position and initial pose of the needle. Further, the needle kinematic model should be modified in order to take into account inhomogeneous tissue and to update particular system parameters such as front wheel offset.

REFERENCES

[1] N. Shahriari, E. Hekman, M. Oudkerk, and S. Misra, "Design and evaluation of a computed tomography (CT)-compatible needle insertion device using an electromagnetic tracking system and CT images," *International Journal of Computer Assisted Radiology and Surgery*, vol. 10, no. 11, pp. 1845–1852, 2015.
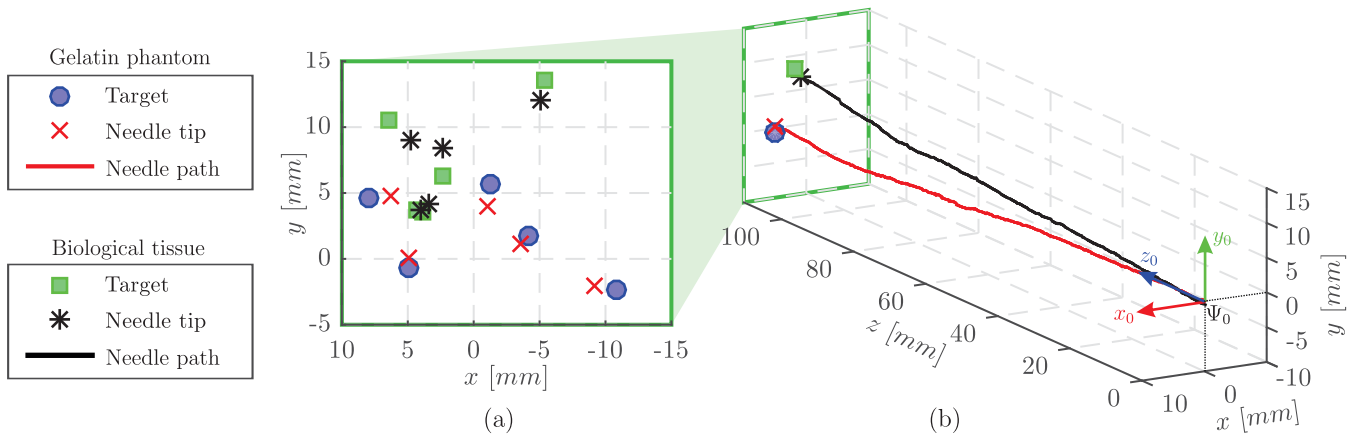
Fig. 6. Experimental results for Case II: (a) The needle is steered towards real targets at different locations in gelatin phantom (Case II.A) and biological tissue (Case II.B) by fusing FBG-sensor data and ultrasound images. Each experiment is performed 5 times. Target positions and actual needle tip positions at target depth are presented in xy-plane. The mean targeting errors are 1.29 ± 0.41 mm and 1.42 ± 0.72 mm for Case II.A and Case II.B , respectively. (b) A representative trajectory of the needle tip for Case II.A and Case II.B in three-dimensional view is demonstrated. The accompanying video demonstrates an example of experimental result for Case II.A-B.

[2] Z. Neubach and M. Shoham, "Ultrasound-guided robot for flexible needle steering," *IEEE Transactions on Biomedical Engineering*, vol. 57, no. 4, pp. 799–805, 2010.

[3] R. J. Webster III, J. S. Kim, N. J. Cowan, G. S. Chirikjian, and A. M. Okamura, "Nonholonomic modeling of needle steering," *The International Journal of Robotics Research*, vol. 25, no. 5-6, pp. 509–525, 2006.

[4] M. Abayazid, G. J. Vrooijink, S. Patil, R. Alterovitz, and S. Misra, "Experimental evaluation of ultrasound-guided 3D needle steering in biological tissue," *International Journal of Computer Assisted Radiology and Surgery*, vol. 9, no. 6, pp. 931–939, 2014.

[5] P. Sears and P. Dupont, "A steerable needle technology using curved concentric tubes," in *IEEE/RSJ International Conference on Intelligent Robots and Systems*, pp. 2850–2856, October 2006.

[6] R. J. Webster III, A. M. Okamura, and N. J. Cowan, "Toward active cannulas: Miniature snake-like surgical robots," in *IEEE/RSJ International Conference on Intelligent Robots and Systems*, pp. 2857–2863, October 2006.

[7] S. Okazawa, R. Ebrahimi, J. Chuang, S. E. Salcudean, and R. Rohling, "Hand-held steerable needle device," *IEEE/ASME Transactions on Mechatronics*, vol. 10, no. 3, pp. 285–296, 2005.

[8] S. Y. Ko and F. Rodriguez y Baena, "Toward a miniaturized needle steering system with path planning for obstacle avoidance," *IEEE Transactions on Biomedical Engineering*, vol. 60, no. 4, pp. 910–917, 2013.

[9] R. J. Roesthuis, N. J. van de Berg, J. J. van den Dobbelsteen, and S. Misra, "Modeling and steering of a novel actuated-tip needle through a soft-tissue simulant using fiber bragg grating sensors," in *IEEE International Conference on Robotics and Automation (ICRA)*, pp. 2284–2289, May 2015.

[10] N. J. van de Berg, J. Dankelman, and J. J. van den Dobbelsteen, "Design of an actively controlled steerable needle with tendon actuation and FBG-based shape sensing," *Medical Engineering & Physics*, vol. 37, no. 6, pp. 617–622, 2015.

[11] J. A. Engh, G. Podnar, D. Kondziolka, and C. N. Riviere, "Toward effective needle steering in brain tissue," in *28th Annual of the IEEE International Conference of Engineering in Medicine and Biology Society (EMBS)*, pp. 559–562, Aug 2006.

[12] M. Abayazid, P. Moreira, N. Shahriari, S. Patil, R. Alterovitz, and S. Misra, "Ultrasound-guided three-dimensional needle steering in biological tissue with curved surfaces," *Medical Engineering & Physics*, vol. 37, no. 1, pp. 145 – 150, 2015.

[13] S. G. Shulman and D. E. March, "Ultrasound-guided breast interventions: Accuracy of biopsy techniques and applications in patient management," *Seminars in Ultrasound, CT and MRI*, vol. 27, no. 4, pp. 298–307, 2006.

[14] L. V. Rodriguez and M. K. Terris, "Risks and complications of transrectal ultrasound guided prostate needle biopsy: a prospective study and review of the literature," *The Journal of urology*, vol. 160, no. 6, pp. 2115–2120, 1998.

[15] M. Abayazid, R. J. Roesthuis, R. Reilink, and S. Misra, "Integrating deflection models and image feedback for real-time flexible needle steering," *IEEE Transactions on Robotics*, vol. 29, no. 2, pp. 542–553, 2013.

[16] H. R. S. Neshat and R. V. Patel, "Real-time parametric curved needle segmentation in 3D ultrasound images," in *IEEE RAS EMBS International Conference on Biomedical Robotics and Biomechatronics (BioRob)*, pp. 670–675, Oct 2008.

[17] P. Chatelain, A. Krupa, and M. Marchal, "Real-time needle detection and tracking using a visually servoed 3D ultrasound probe," in *IEEE International Conference on Robotics and Automation (ICRA)*, pp. 1676–1681, May 2013.

[18] A. Pourtaherian, S. Zinger, P. H. N. de With, H. H. M. Korsten, and N. Mihajlovic, "Gabor-based needle detection and tracking in three-dimensional ultrasound data volumes," in *IEEE International Conference on Image Processing (ICIP)*, pp. 3602–3606, Oct 2014.

[19] G. J. Vrooijink, M. Abayazid, and S. Misra, "Real-time three-dimensional flexible needle tracking using two-dimensional ultrasound," in *IEEE International Conference on Robotics and Automation (ICRA)*, pp. 1688–1693, May 2013.

[20] R. J. Roesthuis, M. Kemp, J. J. van den Dobbelsteen, and S. Misra, "Three-dimensional needle shape reconstruction using an array of fiber bragg grating sensors," *IEEE/ASME Transactions on Mechatronics*, vol. 19, no. 4, pp. 1115–1126, 2014.

[21] M. Abayazid, M. Kemp, and S. Misra, "3D flexible needle steering in soft-tissue phantoms using fiber bragg grating sensors," in *IEEE International Conference on Robotics and Automation (ICRA)*, pp. 5843–5849, May 2013.

[22] A. Othonos, K. Kalli, D. Pureur, and A. Mugnier, "Fibre Bragg Gratings," in *Wavelength Filters in Fibre Optics* (H. Venghaus, ed.), vol. 123 of *Springer Series in Optical Sciences*, pp. 189–269, Springer Berlin Heidelberg, 2006.

[23] J. E. Aldrich, "Basic physics of ultrasound imaging," *Critical care medicine*, vol. 35, no. 5, pp. S131–S137, 2007.

[24] G. Bradski, "The opencv library," *Dr. Dobb's Journal of Software Tools*, 2000.

[25] A. Vaccarella, E. de Momi, A. Enquobahrie, and G. Ferrigno, "Unscented kalman filter based sensor fusion for robust optical and electromagnetic tracking in surgical navigation," *IEEE Transactions on Instrumentation and Measurement*, vol. 62, no. 7, pp. 2067–2081, 2013.

[26] S. J. Julier and J. K. Uhlmann, "Unscented filtering and nonlinear estimation," *Proceedings of the IEEE*, vol. 92, pp. 401–422, March 2004.

[27] A. Gefen and B. Dilmoney, "Mechanics of the normal woman's breast," *Technology and Health Care*, vol. 15, no. 4, pp. 259–271, 2007.